BACHELOR' S THESIS / BIOMEDICAL ENGINEERING 2022

GENERATION OF PERSONALIZED FINITE ELEMENT MODELS OF KNEE JOINT IN A COHORT OF OSTEOARTHRITIS PATIENTS

Clara Ricci

upf. Universitat Pompeu Fabra Barcelona

GENERATION OF PERSONALIZED FINITE ELEMENT MODELS OF KNEE JOINT IN A COHORT OF OSTEOARTHRITIS PATIENTS

Clara Ricci

Bachelor's thesis UPF 2021/2022

Thesis supervisor(s):

Dr. Jérôme Noailly

Universitat Pompeu Fabra Barcelona

Acknowledgments

First, I would like to thank above all my supervisor Jérôme Noailly, PhD for guiding me through the completion of my bachelor's thesis (BT) and for helping me by giving me ideas on how I could proceed, always through his knowledge in biomechanics and finite element modelling.
It has been a difficult year due to the full-time internship, so he has helped me to be constant, to demand tasks from me and to encourage me not to lose motivation and to keep going forward.

Secondly, I would like to thank Dr. Carlos Ruiz Wills and my former colleague Mayra Loayza for jointly explaining Mayra's thesis to me, which would be my starting point, and for offering me their help in resolving my doubts and helping me whenever I had difficulties understanding something about it.

I would also like to deeply thank my friends, especially Angela, Paula, Marta, Marina, Anna, Sergi and Aina for always being by my side and supporting me in both good and difficult times.
Finally, my heartfelt acknowledgements go to my parents, Tono and Lourdes, and my sister, for their unconditional support, encouragement, and constant appreciation of my efforts.

Summary/Abstract

Osteoarthritis (OA) is a highly multifactorial disorder that largely lacks information for proper patient stratification. Its most prevalent form is knee OA. The core pathophysiology of the disorder consists in a dysregulation of articular chondrocyte activity. The later becomes catabolic and contributes to the destruction of the articular cartilage, which eventually generates chronic pain, stiffness, and loss of mobility. Mechanical loads are suspected to participate in the evolution of OA or at least in the evolution of the symptoms. Therefore, detailed descriptions of these loads in the knee joints might be useful to support the objective design of for both prevention and treatment strategies. Arguably, these loads cannot be measured in situ, but Finite Element (FE) models are valuable tools to create patient-specific models and simulate joint mechanics, at both the organ and tissue levels.

Unfortunately, patient-specific modeling of knee joints remains an unmet challenge, mainly because of the complexity of the joint structure and shape, especially in patients affected by OA. Accordingly, the work consists in the generation and analysis of personalized FE models of the knee joints in a clinical cohort of 80 patients acquired in collaboration with the Rheumatology Service of the Hospital del Mar.

An existing Bayesian Coherent Point Drift (BCPD) algorithm was applied to create a personalized 3D FE models of the knee joints of the patients, based on point set registration between a knee joint FE reference model that incorporates a structural mesh with all the tissues found in a healthy joint, and degenerated knee geometries reconstructed out of MRI. The quality of the mesh of the registered source, i.e., morphed, was determined, and used to define a multistep morphing pipeline and adjust the BCPD algorithm parameters.

Keywords

Osteoarthritis; Knee Joint; Patient-Specific Modelling; Computational Biomechanics; Finite Element Modelling; Mesh Morphing; Structural Mesh; Bayesian Coherent Point Drift

Preface

Knee osteoarthritis (OA) is one of the leading causes of adult disability worldwide. It affects more than 16% of the population and it is more common in woman, being 4:1 the female-to-male prevalence ratio. The disease develops slowly, and the main symptom is pain, which worsens over time. There is no cure and patient management is palliative, aiming to treat pain and function, so as to preserve an active and qualitatively satisfactory life.

In a healthy joint, articular cartilage covers and protects the ends of the bones of the joints, so in a joint with osteoarthritis, the cartilage deteriorates over time leaving the bone exposed and generating pain during movement. Clinical decision-making is not an easy task that can be made with objective criteria, but with the help of biomechanics like motion analysis, it would be possible to obtain more accurate and reliable information to understand the development of the disease and influence then, the choice of one treatment or another.
Finite element models can help simulate knee biomechanics which can be informative to determine the state of the tissue and thus help clinical decision-making by establishing a good treatment option suitable for a certain patient.

Nonetheless, the closer the model is to the patient geometry, the better the representation of the tissues can be obtained, and the final clinical decision shall be much better supported.

Index

List of Figures

List of Tables

1. Introduction

1.2 Statement of the problem

Osteoarthritis (OA), the most prevalent chronic joint disease, increases in prevalence with age, and affects majority of individuals over the age of 65 [1]. OA affects 240 million people globally. Worldwide estimates are that 9.6% of men and 18.0% of women aged over 60 years have symptomatic OA [2]. The most affected joints are usually the weight-bearing joints, such as the hip and knee. In fact, hip and knee OA are ranked 13th globally for years life lost due to disability (YLDs) [2].

Ageing changes in the musculoskeletal system increase the propensity to OA but the joints affected, and the severity of disease are also closely related to other OA risk factors such as joint injury, obesity, genetics, and anatomical factors that affect joint mechanics [3].The lack of estradiol is associated with the pathogenesis of OA in postmenopausal women, the inflammatory factors of IL-1, IL-6, TNF-α in postmenopausal increased in serum and synovial fluid may promote and aggravate the OA [4].

Due to the high prevalence of OA, a high economic burden is associated with the disease. It is largely attributable to the effects of disability, the emergence of comorbidities and the expense of treatment [5]. As a chronic disease with pain as the dominant symptom, pain management and restoration of function are insufficient, and OA remains challenging to treat. Joint replacement surgery is the only option left in end-stage disease to increase the quality of life in cases where conventional treatment of symptoms did not provide satisfactory results, making knee arthroplasty in OA as a revolutionary operation and a hallmark of the current impotency of rheumatology-based approaches to cope with OA, medicine, and science at the same time [6].

Static loads have a significant impact for OA development, as they promote chondrocyte malfunction and subsequent apoptosis, but they do not reflect loads generated during locomotion. Movements, angulation, and normal gait produce dynamic loads on joints up to five times body weight in the ankle and up to three times in the knee relative to standing [41]. It is essential to understand how mechanical forces distribute throughout the articular cartilage tissue and change over time in the pathologic joint [45]. Therefore, detailed description of these forces can help the clinical decision-making process of determining prevention and treatment strategies.

Although it is known that biomechanics influences OA's progression, there is not a clear understanding of OA's natural course since it is a multifactorial condition. Finite element models can help simulate knee biomechanics which can be very informative and finite element analysis (FEA) of the human knee joint can help extensively in determining the

underlying causes of cartilage degeneration which in turn results in osteoarthritis [7]. But patient-specific modeling is not sufficiently addressed, since the long time required to generate accurate subject-specific models, with detailed three-dimensional (3D) geometries and feasible FE meshes, may take several working days per patient.

1.2 Statement of purpose

The main purpose of this study is to generate personalized 3D FE model of the patients' knee by employing an efficient, robust, and eventually automatable method. The approach that was specifically targeted is multistep morphing with Coherent Point Drift (CPD) algorithms. The personalization was based on a healthy 3D knee model that includes all soft and bony tissues.

2. State of the art

2.1 The human knee joint

The knee joint is one of the largest joints with a complex structure in the human body and performs a crucial role in many activities of daily living such as standing, walking, running, and climbing stairs [8]. Is the intermediate joint of the lower limb and it allows the movement between the femur, tibia, and patella.
The understanding of anatomy and knee biomechanics is important for the gait analysis, the diagnosis of joint diseases and the design and development of prosthetic implant [9].

2.1.1 Anatomy of the human knee

The knee joint is made up of bones, cartilage, ligaments, and fluids. The two important connecting bones are the femur (distally) and the tibia (proximally), and there is contact with a third small bone, the patella, which articulates with the anterior and inferior portion of the femur.

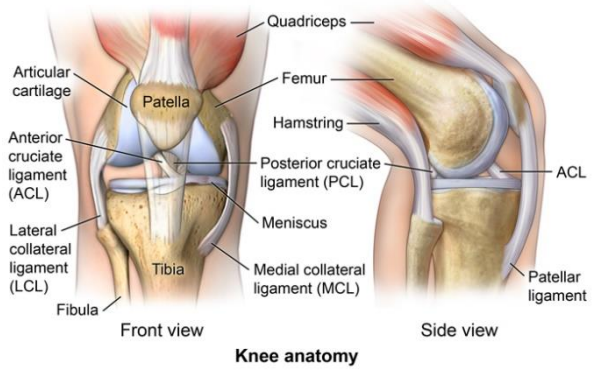

Figure 1: The human knee joint and its components. (From https://www.spectrumhealthlakeland.org/lakeland-neurosurgery/neurosurgery-health-library/Content/85/P07388/)

When the leg is flexed or straightened, the femur rotates over the tibia, while the patella runs along the end of the femur. The stability of the knee is provided by the ligaments that attach to the different bones. The medial collateral ligament (MCL) and lateral collateral ligament (LCL) prevent the femur and tibial plateau from bending outwards or inwards while the anterior cruciate ligament (ACL) and posterior cruciate ligament (PCL) provide additional stabilization so that the tibia is prevented from the anterior-posterior translation.

Given this, the bone surfaces permit six degrees of movement, three translational (anterior-posterior, medial-lateral, and inferior-superior) and three rotational (flexion-extension, intra- external rotation, adduction-abduction) [9]. After all, the movement occurs because of the presence of the meniscus, that provides a cushion between the contact surface of tibia and femur while absorbing the impact forces on the knee joint and providing stability [8].

2.1.2 Articular cartilage

The articular surfaces of the knee are covered by articular cartilage (AC) whose principal function is to provide a smooth, lubricated surface for articulation and to facilitate the transmission of loads with a low frictional coefficient [10].
Articular cartilage is a 1 to 5 mm thick hyaline cartilage, and it consists of a hydrophilic extracellular matrix (ECM) with chondrocytes, collagen, and proteoglycans. Collagen represents a 10-20% of the cartilage weight and the 90% of it its type II collagen, being the responsible to maintain the tensile strength.

The articular chondrocyte is the only cell type in articular cartilage and responsible for generating and maintaining the cartilaginous extracellular environment [11], as well as in

the repair of damaged tissue. Chondrocytes regulate metabolism by a balance of anabolic and catabolic signals in the cartilage. As the cartilage matures, an inadequate response of the extracellular matrix to mechanical loads generates a cascade of catabolic signals that leads to the chondrocyte phenotype changing completely and becoming hypertrophic. The articular chondrocytes will then undergo apoptosis and the articular cartilage will eventually be completely lost. The reduced joint space resulting from total loss of cartilage will cause friction between bones, leading to pain and limited joint mobility [12].

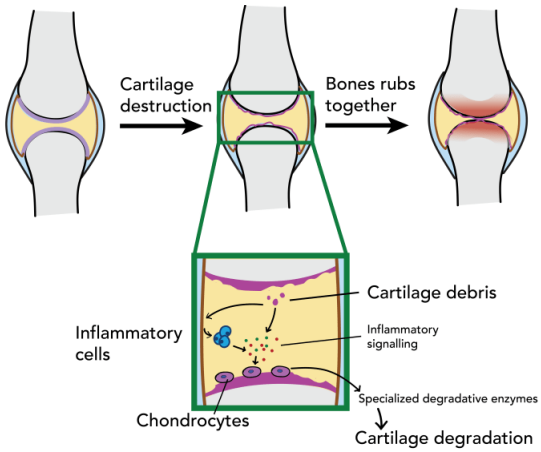

Figure 2: Representation of OA progression and the implication of chondrocytes in the degeneration process. [Treating Osteoarthritis the Smart Way - Science in the News (harvard.edu)]

2.2 Knee Osteoarthritis

Osteoarthritis (OA) is the most common musculoskeletal complaint. Characteristics of OA include articular cartilage degeneration, narrowing of joint space, pain, and loss of function [13].

There are two types of knee osteoarthritis:

- **Primary osteoarthritis:** related to ageing and wear and tear on the bones and cartilage. It usually affects people over the age of 65
- **Secondary osteoarthritis:** usually caused by a previous injury, such as a fracture or a ligament rupture. It usually affects athletes and people who are overweight.

2.2.1 Risk factors and prevalence

Rather than OA being a simple consequence of joint ageing and repeated wear and tear, the current conceptual framework for the relationship between ageing and OA is that ageing of the musculoskeletal system increases the susceptibility to OA but alone does not cause it [14]. The major risk factors for the onset and progression of OA comprise age, gender, genetics, overweightness, joint misalignment, and joint injuries [15].

OA affects 240 million people globally. Worldwide estimates are that 9.6% of men and 18.0% of women aged over 60 years have symptomatic OA [2]. The prevalence of knee OA increased significantly over the last decades and continues to rise, partially because of the increasing prevalence of obesity and other risk factors, but also independently, of other causes [16]. Another significant thing to mention is the economic burden that knee OA brings to the society. According to GBD 2015 Disease and Injury Incidence and Prevalence Collaborators, approximately 85% of the burden of osteoarthritis worldwide relates to knee OA [17].

2.2.1 Diagnosis and treatment

The most common symptom of knee OA is pain, typically occurred when the movement is initiated. Physical examination is important in making the diagnosis. Pain and limitation of range of motion are common to all forms of osteoarthritis, but each joint has unique physical examination findings [18]. These findings should be joint effusion, crepitus (a grating sensation inside the joint) with movement, lateral instability, as well as signs of injury to muscles, tendons, and ligaments surrounding the joint.
Because osteoarthritis is primarily a clinical diagnosis, physicians can confidently make the diagnosis based on the history and physical examination. Plain radiography can be helpful in confirming the diagnosis and ruling out other conditions [19].

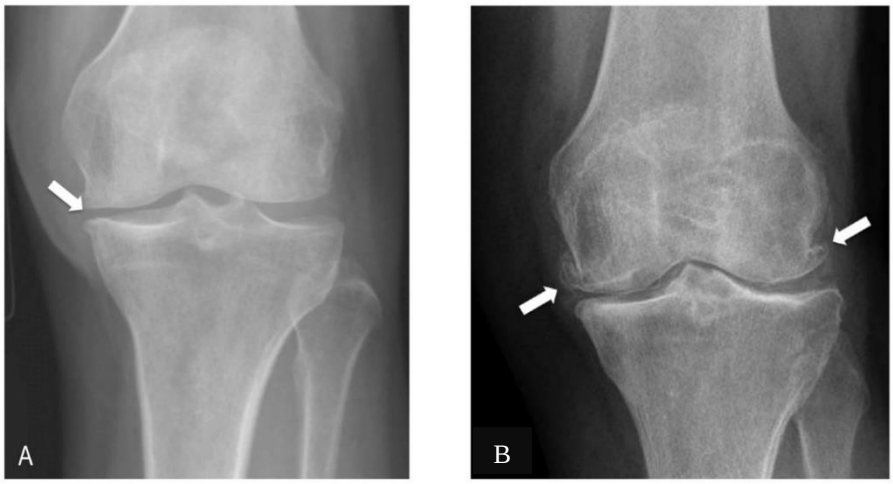

Figure 3: Anterior-posterior (AP) radiograph of a left knee with A) mild osteoarthritis, where the arrow indicates joint space narrowing and B) moderate or severe osteoarthritis, where the arrows indicate joint space narrowing and possible bone deformation. [Knee Osteoarthritis: A Primer - PMC (nih.gov)]

Other imaging studies, such as magnetic resonance imaging, computed tomography, or a bone scan, although usually not required, may be needed to rule out other conditions of the bone and soft tissues of the joint [20].
Despite the prevalence of OA, it is only in recent years that considerable progress has been made in the understanding of the disease. Yet, transferring such knowledge to the

clinical management of joint degenerations remains a major challenge, because of the complex multiscale interplays among joint morphology, joint biomechanics, chondrocyte mechanobiology, and biological signaling. Hence, prevention strategies and therapeutic measures employed to date are insufficient to cure knee OA, and current treatments are palliative targeting pain and function without being able to revert or even stop the progression of the disease.

Treatment choices fall into four main categories: nonpharmacologic, pharmacologic, complementary, and alternative, and surgical [18]. As a chronic disease with pain as the dominant symptom, pain management and lifestyle changes are insufficient, and OA remains challenging to treat. Joint replacement surgery is the only option left in end-stage disease to increase the quality of life in cases where conventional symptomatic treatment did not provide satisfactory results, making knee arthroplasty in OA as a revolutionary operation and a defeat of orthopedics, medicine, and science at the same time [6].

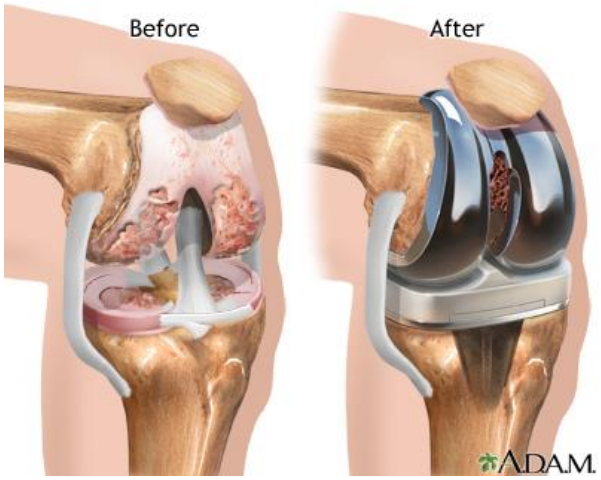

Figure 4: Representation of knee status before and after total knee joint replacement with arthroplasty surgery [From *Knee joint replacement: MedlinePlus Medical Encyclopedia]*

2.3 Patient-specific 3D finite element modeling

Due to the patient-specific nature of the disease, predicting its progression is extremely challenging. Therefore, there is an unmet need for clinical tools that would give answers to two questions [21]:

1- Will the current knee joint state and physical activity habits lead to severe OA?
2- If yes, can OA be prevented or its progression delayed by conservative treatments (e.g., weight loss, gait retraining, physical exercise)?

Finite Element Method (FEM) is one of the computational techniques that has been extensively adopted to study the biomechanics of the knee joint [22]. Thus, it assesses the relationship between load carrying functions and morphology of the tissues [46], as these

loads cannot be measured in situ. Hence, a Finite Element Analysis (FEA) can help to determine the main causes of cartilage degeneration that will led into OA.

To carry out an FEA, a 3D FE model is needed, which is obtained by reconstructing a medical image, usually an MRI, followed by the generation of a computable mesh. Often the latter needs to be structural, i.e., discretization must respect tissue structure, imposing the achievement of delicate trade-offs between geometrical modelling and mechanical simulation capacity. For knee joint FEAs, the time required to generate accurate subject-specific models, with detailed three-dimensional (3D) geometries and feasible FE meshes, is the main drawback for clinical implementation, since it may take several working days and tedious manual modelling, per individual [23]. The reason it takes so long is because of the geometry of the soft tissues of the OA knee are often shattered or completely missing. Upfront, the soft tissue segmentation process becomes very challenging as traditional threshold and/or region growing methods lack robustness in the context of osteoarthritic knees. Furthermore, the finite element modelling of structurally damaged tissues, with structural meshes, leads to unmanageable mesh distortions for finite element solvers. Therefore, building patient-specific 3D models of the knees of OA patients is utmost challenging.

An alternative is to generate generic models with simplified geometries which can later be morphed or transformed into each individual patient's shape [24].
Mesh morphing is defined as a method for changing the shape of a meshed surface while preserving the topology. Only node positions are updated [25] and the ultimate goal is to obtain a transformation of a source model with the target geometry.
Mesh morphing is based on a point set registration, which is intended to find correspondences and estimate the transformation (rotation and translation) between two or more point sets [26].

Typically, registration algorithms are categorized as either rigid or non-rigid according to the transformation models that deform shapes and align them. Rigid registration algorithms find a map that preserves the distance between every pair of points, i.e., a map defined as rotation and translation [27]. In contrast, non-rigid registration algorithms find a map that does not necessarily preserve the distance between points [27].
In an in-house study performed by Weng previous to this Bachelor's Thesis, a combination of rigid transformation and non-rigid transformation was used with the iterative closest point (ICP) and thin plate spines (TPS) algorithms, respectively [28].

The ICP, introduced by Besl and McKay [29] and Zhang [30], is a well-known method in the field of point set registration for rigid transformation between two points. The ICP is an algorithm used to minimize the difference between two sets of points [29] and its key feature is that it works with an automatic point correspondence, it iteratively associates points by the nearest neighbor criteria minimizing a cost function [31].
The TPS algorithm is a non-rigid transformation that uses interpolation to align previously defined landmark points. Bookstein et al. [32] pioneered the use of TPS to

generate smooth spatial mappings between two sets of points with known one-to-one correspondences (landmarks) in medical images.

As a result of Weng's study [28], the combination of both algorithms led to accurate shape deformations but there were critical errors on the resultant finite element mesh because of geometric irregularities, probably due to damaged tissue because of OA. Hence, alternative approaches are needed to cope with the negative impact of OA-specific tissue irregularities.

In this study, we hypothesize that soft tissue disruption can be considered through the alteration of local model tissue parameters during the biomechanical modelling. Accordingly, simulated tissue damage becomes independent of the geometry, allowing to work with personalized structural meshes, where soft tissues are interpolated to achieve a regular representation of their geometries as if they were healthy. To this aim, the use of another point set registration algorithm, i.e., the Bayesian Coherent Point Drift (BCPD), was explored.

3. Materials and Methods

3.1 Dataset

The dataset is obtained from the HOLOA's project, a collaboration project between Hospital del Mar and Pompeu Fabra University, which its main goal is to design a predictive and exploratory model that considers the 3 main areas implicated in the OA pathology. For that, several patients with knee OA volunteered to take MRI images.
Images of the knee joint were acquired using a T1-weighted with fat-suppressed MRI sequence. Each image has 212 sagittal slices with a resolution of 512x512 pixels and a slice thickness of 0.5 mm. There were 27 knees available, being the left knee of a patient the one selected since the FE model of the knee provided (source model for the mesh morphing) corresponded to a left lower limb.

3.2 Finite Element Model of the healthy knee joint

A 3D FE model of the human knee joint is acquired from the Open-knee database [33] and its mesh was refined afterwards to ensure mesh convergence. It corresponds to a healthy left knee joint consisting of bones, (femur and tibia) soft tissues (the articular cartilage, the lateral and medial collateral ligaments (the LCL and MCL, respectively), anterior and posterior cruciate ligaments (the ACL and PCL, respectively)) and finally the menisci (medial and lateral).

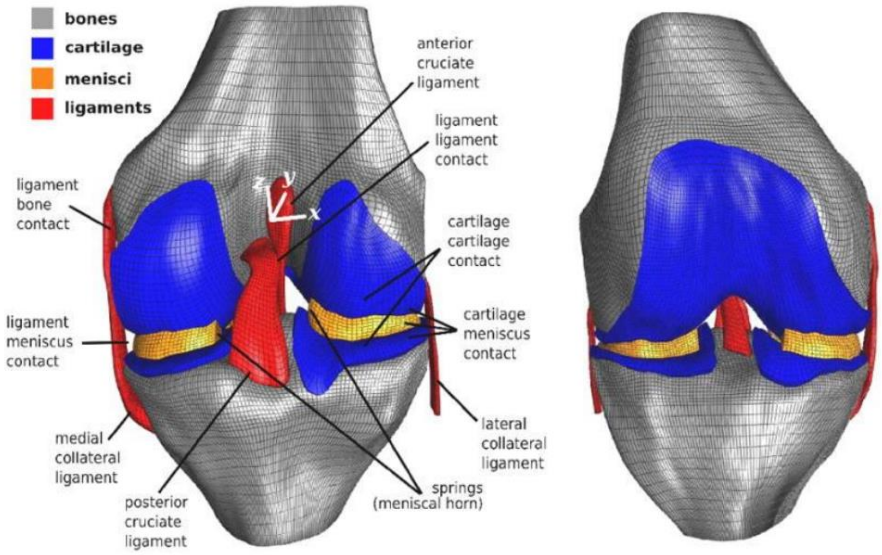

Figure 5: Representation of tibiofemoral joint anatomy and mechanics. All model components are defined on the posterior view of the model, which can be seen on the left. The geometries of bones, cartilage, menisci, and ligaments were individualized to the specimen and discretized into meshes. An anterior view of the whole mesh can be seen on the right [33].

3.3 Pipeline

The created workflow is represented in Figure 6, and consists of the following steps:

1- Segmentation (3D Slicer)
2- Pre-processing of the files: volumetric mesh generation, from STL to VTK (Gmsh)
3- Multistep mesh morphing (Matlab – BCPD Algorithm)
    a. Generation of point cloud for both source and target models (healthy knee joint model and segmented knee joint model, respectively)
    b. Alignment of both point clouds with rigid registration (BCPD algorithm) and correction of the segmented model dimensions
    c. Non-rigid registration (BCPD algorithm) to obtain transformation of source model into target model geometry
    d. Rigid registration (BCPD algorithm) to align original healthy knee joint model and transformed model
4- Mesh Verification (Abaqus CAE)

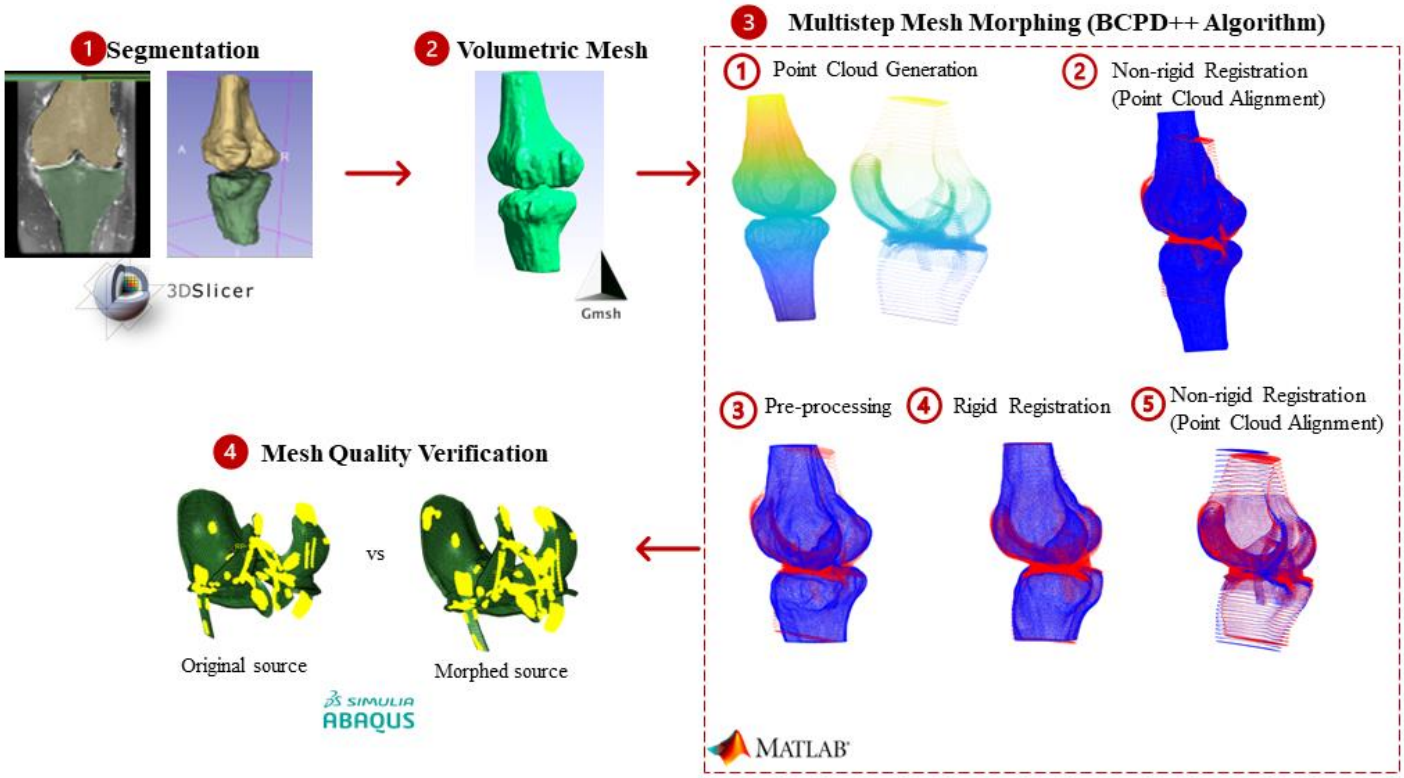

Figure 6: Pipeline followed during the development of the BT and the software used in every step of the process.

3.3.1 Segmentation

The images of the patients are segmented using the open access 3DSlicer software with default values. Only the bones, femur, and tibia, are segmented, as each segmentation will be the target model for the mesh morphing and the bones are the ones that mainly define the geometry of the joint.

STL is the exported format, and it describes surface geometry of a 3D object without any color, texture, or other attributes. This format uses a series of linked triangles to recreate or reproduce surface geometry of the 3D model [34].

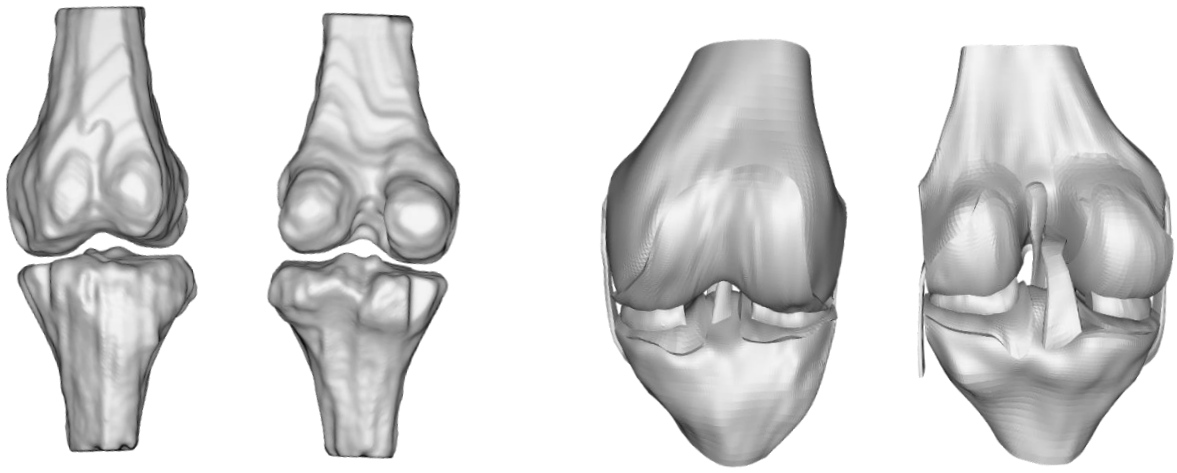

Figure 7:Posterior and anterior view of A) Segmentation of the knee joint from images of an actual patient with knee OA and B) 3D finite element model of the human knee joint, including the bones, the articular cartilages, the ligaments, the lateral meniscus, and the medial meniscus, visualized in Abaqus

3.3.2 Pre-processing of the files

Once we have the segmented models in STL, they are converted to VTK with the Gmsh software to obtain information about the nodes and cells of the model that form the geometry.

If opening the file with a notepad it can be distinguish the basic structure of the VTK and the only part that is needed for this study is the fourth part, which contains the mesh structure. It contains the points and the topology. This part begins with a line containing the keyword DATASET followed by a keyword describing the type of dataset [35].

The healthy FE model file of the knee was initially in input format generated in Abaqus CAE. To carry out mesh morphing, both models must have the same format, so the input file must be converted to VTK. There is no direct conversion, it first must be converted to a Nastran input file (known as a bulk data file (.BDF)) with the Abaqus CAE software. Afterwards, it is imported into Gmsh and exported in VTK format.

Finally, the two files needed for mesh morphing are already in the same format, the healthy FE model will be the source and the segmented model will be the target.

3.3.3 Multistep mesh morphing with BCPD algorithm

As mentioned in section 2.3, mesh morphing is a method for changing the shape of a meshed surface while preserving the topology [25] and the goal of point set registration is to find pairs of corresponding points between shapes represented as point sets.

In this study, an algorithm based on point set registration called Bayesian Coherent Point Drift.

Coherent point drift (CPD) [36], is a collection of three different registration algorithms based on a Gaussian mixture model (GMM). CPD is considered a state-of-the-art non-rigid registration algorithm because of its registration performance and scalability to large point sets [37]. Despite the advantages of CPD over state-of-the-art algorithms, several issues remain in both theoretical and practical aspects [27]. One theoretical issue of CPD is that it is unknown whether the algorithm always converges, as suggested by Myronenko et al. [47]. In a practical aspect, CPD is relatively sensitive to the rotation of a target [27] and it has a high computational cost that cannot be overcome due to the limitation of CPD to the case of the Gaussian function.

Hirose (2020) [27] formulates CPD in a Bayesian setting that addresses both theoretical and practical issues by replacing the motion coherence theory, i.e., the theoretical basis of CPD, with Bayesian inference; and introduces motion coherence using a prior distribution of displacement vectors. With this:

- Convergence of the algorithm is guaranteed.
- The parameters regarding motion coherence can be interpreted intuitively.
- The algorithm combines the rigid CPD and the non-rigid CPD.
- The algorithm can be accelerated with non-Gaussian kernel functions.

Bayesian formulation of CPD

Hirose (2020) [27] formulated CPD in a Bayesian setting; introduced motion coherence using the prior distribution of displacement vectors rather than using the motion coherence theory. He supposes that $T(y_m)$ is the function that deforms the shape represented as Y to match it with the shape represented as X.

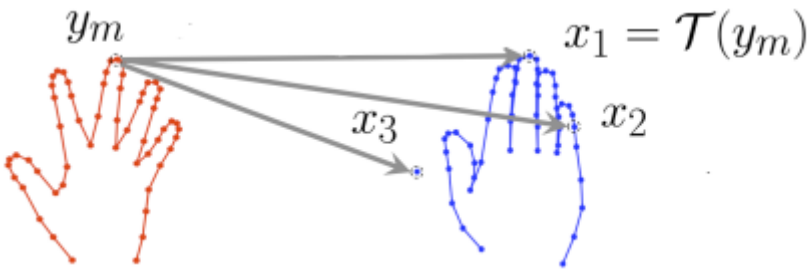

Figure 8: Representation of the displacement vectors between the source point set (red) and the target point set (blue). From [27].

He also derived BCPD registration algorithm, which is interpreted as a generalization of the CPD algorithm, using Variational Bayesian inference (VBI). The Bayesian formulation provided a clear difference between tuning parameters controlling the motion coherence. [27].

The tuning parameters are, then:

1. Omega (w) [0,1]: controls the outlier probability

2. Lambda (λ) > 0: controls the expected length of displacement vectors. Smaller is longer
3. Beta (β) > 0: controls the directional correlation between displacement vectors, i.e, it controls the range where deformation vectors are smoothed.
4. Gamma (γ) > 0: it defines the randomness regarding the initial guess of point matching
5. Kappa (κ) > 0: it controls the uniformity of the number of target points matching with a source point

It is important to keep in mind that, according to Hirose's study [27] one issue of CPD is the difficulty in interpreting tuning parameters λ and β. Both parameters control the degree of motion coherence but tend to be controlled in a non-intuitive manner. In this study, only the variations of lambda and beta will be studied to predict an optimal combination of both to obtain a good mesh morphing between the source and the target.

We can interpret the values of lambda and beta according to the following scheme:

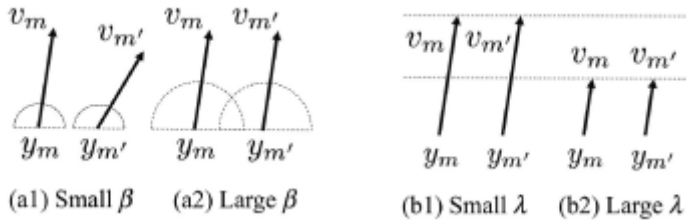

Figure 9: Interpretation of tuning parameters β and λ: a) β controls the directional correlation between displacement vectors and b) λ controls the expected length of displacement vectors. From [27].

In a way that, β will be very sensitive to the angles so if a small β is chosen, the deviation of the angles between displacement vectors will be higher. For λ, on the other hand, the smaller the value, the larger the displacement vector and the greater the deformation the source undergoes to adapt to the target geometry.

Point set registration algorithms can be classified into hard and soft matching on the basis of the decision procedure for point-to-point correspondences between two shapes [38]. One issue with the soft-matching methods is their computational costs; they require affinity computations involving all pairs of points between two shapes. [38].

To address this issue, Hirose (2021) propose an acceleration method (BCPD++) for non-rigid point set registration. The method, accelerates non-rigid registration via:

1. Down sampling of point sets
2. Non-rigid registration of the down sampled point sets using the BCPD algorithm
3. Interpolation of shape deformation vectors corresponding to the removed points

BCPD++ requires the same tuning parameters as BCPD, because it uses BCPD as the registration algorithm. During this thesis, only effects of lambda and beta parameters when changing were studied.

If λ is sufficiently large (around 10^9), the BCPD++ algorithm solves rigid registration problems [39], that is, deformation of the source shape is minimum because it preserves the distance between every pair of points, i.e., a map defined as rotation and translation [27].

3.3.4 Mesh Verification

After multistep morphing is completed, the result is an *input* format file of a morphed source with the geometries of a target patient. The quality of the resultant morphed mesh needs to be verified to obtain information about the nodes and elements. ABAQUS/CAE highlights any elements that fail the mesh quality tests and displays the number of elements tested along with the number of errors and warnings in the message area. At a minimum, the mesh quality tests issue a warning for elements that seem inappropriately distorted, and the tests issue an error if the distortion is severe [40].

The software will highlight elements according to the following selection criteria and their limits (Table 1) [40]:

- **Smaller face corner angle:** ABAQUS/CAE highlights elements containing faces where two edges meet at an angle smaller than a specified angle.
- **Larger face corner angle:** ABAQUS/CAE highlights elements containing faces where two edges meet at an angle larger than a specified angle.
- **Aspect ratio:** ABAQUS/CAE highlights elements with an aspect ratio larger than a specified value. The aspect ratio is the ratio between the longest and shortest edge of an element.
- **Short edge:** ABAQUS/CAE highlights elements with an edge shorter than a specified value.
- **Shape factor:** ABAQUS/CAE highlights elements with a normalized shape factor smaller than a specified value. The shape factor criterion is available only for triangular and tetrahedral elements.
    - For triangular elements: $shape\ factor = \frac{element\ area}{optimal\ element\ area}$
    - For tetrahedral elements: $shape\ factor = \frac{element\ volume}{optimal\ element\ volume}$

      Where optimal element area/volume is the area/volume of an equilateral triangle/tetrahedron with the same circumradius as the element, respectively.

Selection criteria limits	Type of mesh elements				
	Quadrilateral	**Triangular**	**Hexahedral**	**Tetrahedral**	**Wedge**
Smaller face corner angle	<10	<5	<10	<5	<10
Larger face corner angle	>160	>170	>160	>170	>160
Aspect ratio	>10	>10	>10	>10	>10
Short edge	<0.01	<0.01	<0.01	<0.01	<0.01
Shape factor	N/A	<0.01	N/A	<0.0001	N/A

Table 1: Default selection criteria limits of Mesh Verification tool in Abaqus CAE. From [40].

4. Results

4.1 Multistep Morphing

1) First step of the multistep morphing: Rigid Registration

BCPD++ becomes a rigid registration if λ goes to infinity ($\lambda = 10^9$), besides this, default values of the tuning parameters were used: $(\omega, \lambda, \beta, \gamma, \kappa) = (0.2, 10^9, 2, 10, 70)$.

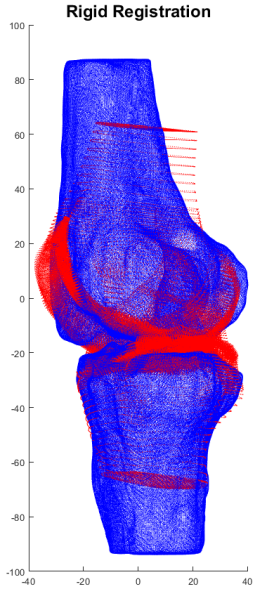

Figure 10: Result of first step of multistep morphing, a rigid registration. The blue point cloud is the segmented knee of patient 40 (target) and the red point cloud is the healthy knee (source).

The result of the rigid registration, as we can see, is a simple alignment of the source and the target to later correct the dimensions of the target according to those of the source, that is to say, to eliminate the excess femur and tibia.

After some pre-processing and correction of the target dimensions, the point sets with which we will do the non-registration are:

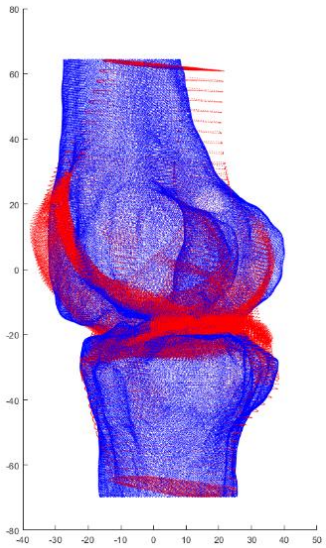

Figure 11: Pre-processing of the blue point cloud (target) so that it matches the dimensions of the red point cloud (source).

2) Second step of the multistep morphing: Non-Rigid Registration

The first results are obtained with the default values of the tuning parameters $(\omega, \lambda, \beta, \gamma, \kappa) = (0{,}50{,}2{,}10, \infty)$ Hirose [27] used in his study.

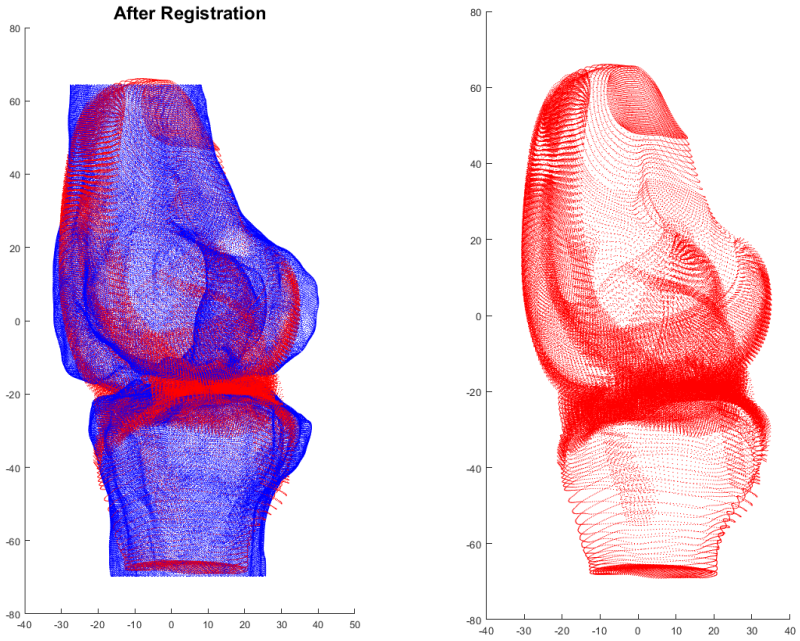

Figure 12: First results of the rigid registration where red point cloud *is the morphed source to match the target geometry (blue* point cloud*).*

After looking at the results, the source has not adjusted well to the geometry of the target and that the algorithm has deformed the upper part of the tibia too much. It is concluded that the beta is too low, so it is too sensitive, and the deviation of the angles is too large. New value for beta is defined, $\beta = 2.9$ (maximum $\beta = 3.0$), and the new registrations are more accurate than the previous.

The results are evaluated with the root mean square error (RMSE) returned as a positive value, which measures the Euclidean distance between the aligned point clouds, that is, measuring the similarity across the post-registration point cloud and the target point cloud (ground truth) [48]. In this case, only the bones of the post-registration point cloud were considered since the ground truth didn't have the soft tissues. The lower the RMSE, the smaller the error and the more accurate the registration, i.e., the better the morphed source fits the geometry of the target.

It is important to say that the RMSE shown is the modulus of RMSEx, RMSEy and RMSEz, thus, the unit is mm, so if we consider that the target measurements are:

$$XLimits: [-15.2194, 56.9548]mm$$
$$YLimits: [-51.1033, 14.2601]mm$$
$$ZLimits: [31.1949, 157.1331]mm$$

Then, RMSE values of Table 2 are relatively small compared to the model measurements.

Several rigid registrations are made for different patients, leaving beta constant and varying lambda.

	Morphed Source with **Patient 028**	Morphed Source with **Patient 143**	Morphed Source with **Patient 120**	Morphed Source with **Patient 008**	Morphed Source with **Patient 040**
$\lambda = 50$ $\beta = 2.9$	RMSE = 50.8856	RMSE= 53.2199	RMSE = 55.1353	RMSE = 54.6437	RMSE = 57.3489
$\lambda = 100$ $\beta = 2.9$	RMSE = 50.7679	RMSE = 53.4866	RMSE = 55.1822	RMSE = 54.5044	RMSE = 57.2773
$\lambda = 200$ $\beta = 2.9$	RMSE = 50.4629	RMSE = 53.1028	RMSE = 54.9556	RMSE = 54.2771	RMSE = 57.1649
$\lambda = 300$ $\beta = 2.9$	RMSE = 50.6811	RMSE = 53.5352	RMSE = 54.9355	RMSE = 54.4959	RMSE = 56.9223
$\lambda = 400$ $\beta = 2.9$	RMSE = 50.3714	RMSE = 53.1267	RMSE = 54.8056	RMSE = 54.3365	RMSE = 56.8702

Table 2: RMSE for patients' number 028, 143, 120, 008 and 040, fixed β value at 2.9 and increasing λ value from 50 to 400.

The results do not show much difference to the naked eye with a lambda of 50 and a lambda of 400, which is why the RMSE must be used to identify which rigid registration is the most accurate.

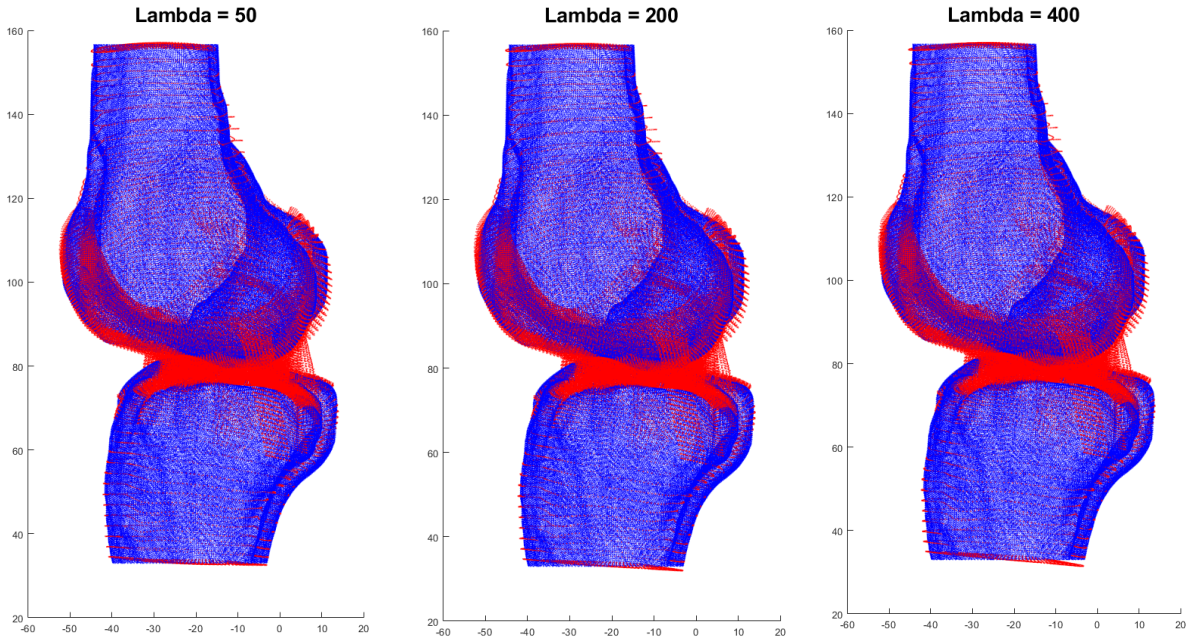

Figure 13: Non-rigid registration of the original source point set and the target point set (patient 143) which results in a morphed source (red) point set adapted to the target geometries.

At first glance it might seem that the morphed source that has best adapted to the geometry of the target is the lambda 50, as the only apparent difference between the other two is the lower part of the tibia, where the figure of lambda 50 has the most overlap between the two models.
But if we look at the RMSE values, we see that the lowest value is the RMSE and therefore, that should be the most accurate rigid registration result.

3) Third step of the multistep morphing: Rigid Registration

We repeat the first step of the multistep morphing, which consists in a rigid registration to align two models. In this case, the two models to be aligned are the original source and the morphed source, so that the deformation of the former to become the latter can be seen.

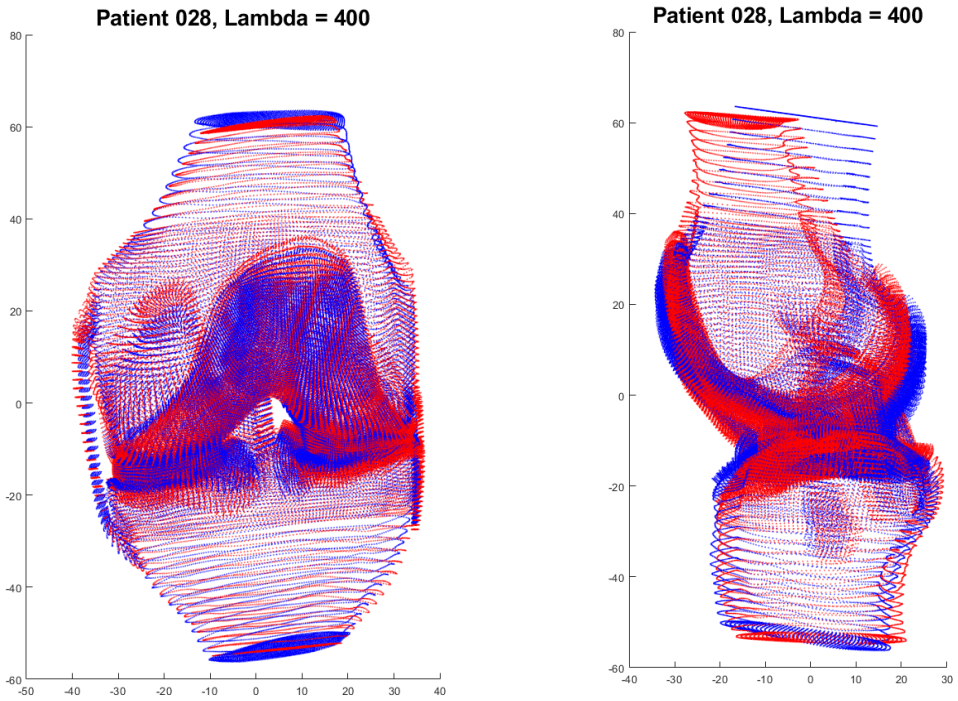

Figure 14: Rigid Registration of the original source point set (blue) and the morphed source point set (red) of patient 028 with $\lambda = 400$.

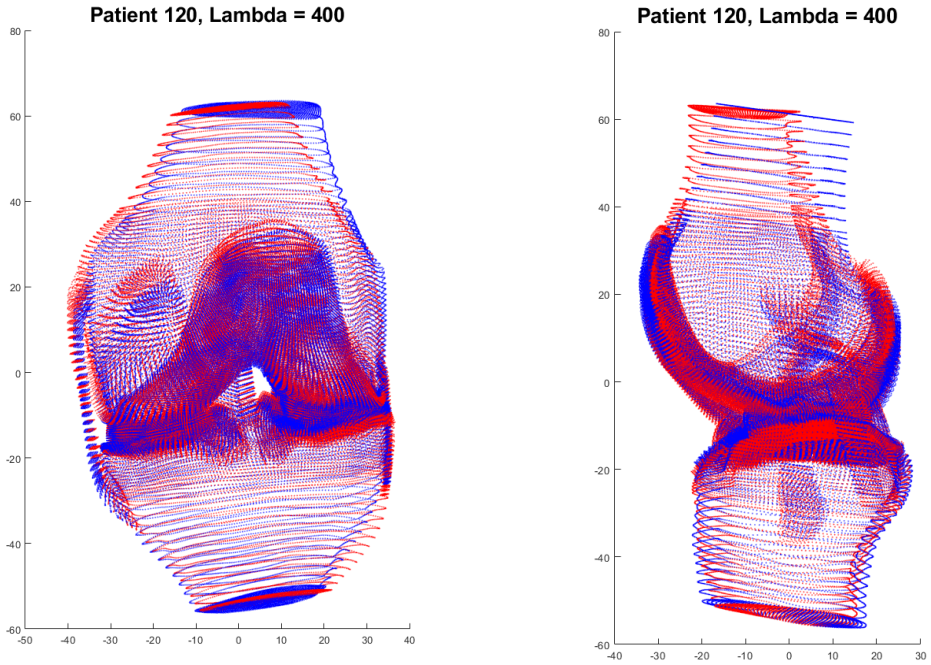

Figure 15: Rigid Registration of the original source point set (blue) and the morphed source point set (red) of patient 120 with λ = 400.

4.2 Mesh Verification

The RMSE is not sufficient to determine an optimal lambda, as it may be that the mesh resulting from the morphed source model contains irregularities and results in a non-computable mesh.
As mentioned in section 3.3.4, the mesh quality tests issue a warning for elements that seem inappropriately distorted considering the selection criteria given in Table 1.

Therefore, the mesh must be verified in Abaqus CAE and compared with the original source. The best mesh will be the one with the least number of analysis warnings in comparison with the original source number, resulting in a structural mesh with the least irregularities.

Tables of analysis warnings after mesh verification in Abaqus CAE:

Morphed Source with **Patient 028**	Original Source	$\lambda = 50$ $\beta = 2.9$	$\lambda = 100$ $\beta = 2.9$	$\lambda = 200$ $\beta = 2.9$	$\lambda = 300$ $\beta = 2.9$	$\lambda = 400$ $\beta = 2.9$
ACT Lateral	568	671	492	444	752	479
ACT Medial	42	172	219	186	156	114
ACF	176	1333	791	353	278	178
CPL	147	125	121	114	120	116
Meniscus Lateral	125	198	182	137	113	111
LL	180	274	267	256	266	252
CAL	140	156	166	158	151	154
Meniscus Medial	117	121	126	121	128	105
LM	289	385	364	345	373	314
Total	1784	3435	2728	2114	2337	1823

Table 3: Number of analysis warnings in every soft tissue after testing mesh quality of every morphed source model with patient 028 created for different λ values with Mesh Verification tool in Abaqus CAE.

Morphed Source with **Patient 143**	Original Source	$\lambda = 50$ $\beta = 2.9$	$\lambda = 100$ $\beta = 2.9$	$\lambda = 200$ $\beta = 2.9$	$\lambda = 300$ $\beta = 2.9$	$\lambda = 400$ $\beta = 2.9$
ACT Lateral	568	574	508	572	571	593
ACT Medial	42	144	260	86	72	68
ACF	176	489	2055	515	516	514
CPL	147	148	196	152	151	153
Meniscus Lateral	125	118	226	133	133	131
LL	180	256	230	237	233	239
CAL	140	172	175	170	169	169
Meniscus Medial	117	96	129	101	102	105
LM	289	383	370	367	362	367
Total	1784	2380	4149	2333	2309	2339

Table 4: Number of analysis warnings in every soft tissue after testing mesh quality of every morphed source model with patient 143 created for different λ values with Mesh Verification tool in Abaqus CAE.

Morphed Source with **Patient 120**	Original Source	$\lambda = 50$ $\beta = 2.9$	$\lambda = 100$ $\beta = 2.9$	$\lambda = 200$ $\beta = 2.9$	$\lambda = 300$ $\beta = 2.9$	$\lambda = 400$ $\beta = 2.9$
ACT Lateral	568	608	467	417	396	386
ACT Medial	42	132	117	94	86	74
ACF	176	1416	989	800	706	640
CPL	147	151	147	146	145	146
Meniscus Lateral	125	195	212	180	166	156
LL	180	271	261	250	240	234

CAL	140	157	158	158	155	154
Meniscus Medial	117	125	118	119	116	114
LM	289	410	388	374	363	352
Total	1784	3465	2857	2538	2373	2256

Table 5: Number of analysis warnings in every soft tissue after testing mesh quality of every morphed source model with patient 120 created for different λ values with Mesh Verification tool in Abaqus CAE.

Morphed Source with **Patient 008**	Original Source	λ = 50 β = 2.9	λ = 100 β = 2.9	λ = 200 β = 2.9	λ = 300 β = 2.9	λ = 400 β = 2.9
ACT Lateral	568	744	697	643	628	627
ACT Medial	42	207	234	222	213	199
ACF	176	1100	474	329	257	209
CPL	147	164	154	141	137	137
Meniscus Lateral	125	216	205	168	155	146
LL	180	268	257	249	241	239
CAL	140	162	164	158	155	152
Meniscus Medial	117	112	117	123	125	126
LM	289	414	393	379	368	365
Total	1784	3387	2695	2421	2279	2200

Table 6: Number of analysis warnings in every soft tissue after testing mesh quality of every morphed source model with patient 008 created for different λ values with Mesh Verification tool in Abaqus CAE.

Morphed Source with **Patient 040**	Original Source	λ = 50 β = 2.9	λ = 100 β = 2.9	λ = 200 β = 2.9	λ = 300 β = 2.9	λ = 400 β = 2.9
ACT Lateral	568	544	511	484	473	467
ACT Medial	42	486	402	343	300	266
ACF	176	3170	1907	1118	839	704
CPL	147	174	162	151	149	148
Meniscus Lateral	125	444	400	348	317	291
LL	180	257	253	246	241	238
CAL	140	181	176	172	169	165
Meniscus Medial	117	168	170	163	154	149
LM	289	434	411	403	400	393
Total	1784	5858	4392	3428	3042	2821

Table 7: Number of analysis warnings in every soft tissue after testing mesh quality of every morphed source model with patient 040 created for different λ values with Mesh Verification tool in Abaqus CAE.

	Morphed Source with **Patient 028**	Morphed Source with **Patient 143**	Morphed Source with **Patient 120**	Morphed Source with **Patient 008**	Morphed Source with **Patient 040**
Minimum RMSE	$\lambda = 400$	$\lambda = 200$	$\lambda = 400$	$\lambda = 200$	$\lambda = 400$
Minimum Analysis warnings	$\lambda = 400$	$\lambda = 300$	$\lambda = 400$	$\lambda = 400$	$\lambda = 400$

Table 8: *Table combination of best values of λ according to the minimum RMSE and minimum number of analysis warnings on the previous tables.*

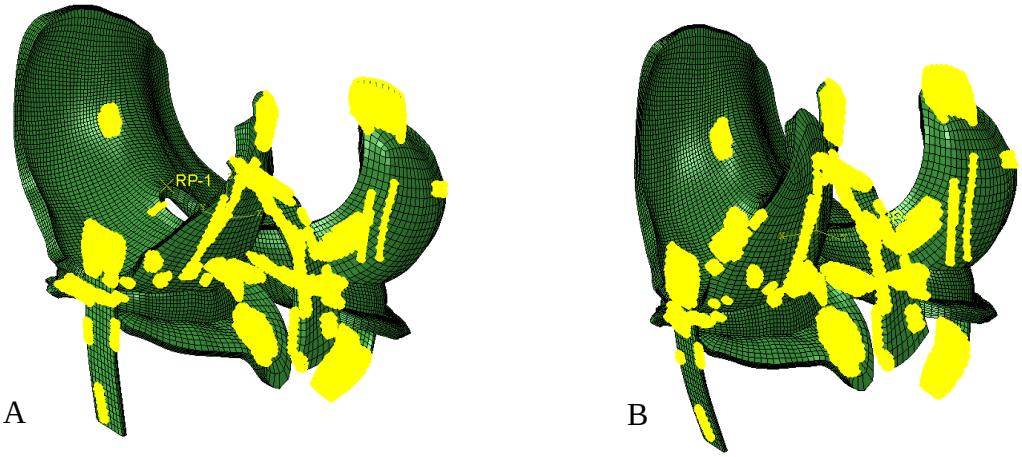

Figure 16: Result after mesh verification in Abaqus CAE where warning elements of the soft tissues are highlighted in yellow. A) Mesh quality of the soft tissues of the healthy knee FE and serves as a reference quantity and distribution of warning elements model. B) Mesh quality of the soft tissues of a morphed FE model of patient 028.

5. Discussion

The main objective of this thesis was to obtain a personalized 3D model of a human knee joint based on a multistep morphing between a healthy knee joint and an osteoarthritic knee joint obtained from a segmentation of an MRI image of a real patient. A patient suffering from knee osteoarthritis has badly damaged soft tissues, so getting a patient-specific 3D model and then being able to predict a treatment or method of action for that patient is practically impossible, as you cannot segment tissue that may not exist.

Computational analyses in biomechanics and medicine are valuable for surgery planning, medical device design, and understanding and preventing disease progression [42].
For knee tissue biomechanics, initial studies focused on structural characterization and mathematical description utilizing simple loading conditions. Then, due to improvements in equipment, increasing computing capacity, and theoretical enrichment, more realistic

geometries and loading conditions were included in the numerical models. Thus, the route from the first 3D knee joint model until now has been a long 40-year journey [43].

Recent studies like Weng's [28], have shown that the acquisition of patient-specific models is becoming more challenging every day because of soft tissues degeneration (See segment 2.3). Also, Papaioannou, et al [49] states that as a consequence of the relative dearth of precise patient-specific geometric data, material properties and relatively inaccurate in vivo kinematics for input, no patient-specific computational models have been reported for longitudinal clinical joint studies.

All efforts are being made to model the knee joint in a more patient-specific way, but it is increasingly clear that the pathology makes this very challenging. Hence, in this study, a new approach to replace patient-specific modeling was presented, personalized modeling.
As shown in segment 3.3.3, BCPD algorithm based on different mesh-morphing techniques, was used to obtain personalized 3D FE models.

Therefore, mesh-morphing is a technique to change an existing geometry or an existing FEM mesh by applying a specific distortion [44]. In this study, a healthy knee 3D FE model constituted by soft and bony tissues was morphed into the osteoarthritic 3D knee geometry defined only by its bones.
For this purpose, two finite element models are used, the first, a healthy knee 3D FE model obtained from Open Knee [33] and subsequently re-meshed to ensure mesh convergence, shown in Figure 5, and the second, a knee segmentation from patients with knee osteoarthritis who volunteered to participate in the HOLOA project, shown in Figure 7. All in all, it can be said that the objective of the thesis has been met and the results are quite promising, although there is still work to be done.

Morphing is performed with BCPD++ algorithm and it is done in three steps: rigid registration, non-rigid registration, and rigid registration, as shown in Figure 6. This algorithm is used to obtain a personalized model for each patient and to replace the approach made by the ICP and TPS algorithm, which, as seen in the literature [28], have many limitations and it is arguably not possible to obtain a patient-specific model with them.

Before the non-rigid registration of the algorithm, an initial rigid registration and pre-processing was needed to perform some corrections on the target model. As a result of the first rigid registration, it can be seen in Figure 10 that the target's femur and tibia are quite larger than the source ones, so dimensions were fixed and shown in Figure 11.

The algorithm for non-rigid registration was initially used with the default parameters [39] and the results, which can be seen in Figure 12, show that the original source does indeed adapt to the geometry of the target but there are many irregularities. First, the upper part of the femur is completely bent, which is not physically possible, then the soft

tissues are too deformed, the articular cartilage becomes overly elongated, which also does not make sense as it should in any case become smaller, following the logic of what happens to the articular cartilage as OA progresses.

If we look at Figure 9, we see that one of the two parameters (β) of the algorithm tends to skew the angles of the displacement vectors more than necessary. According to the study [27], the smaller the β, the more the model is deformed. The algorithm is run for larger β until $\beta = 2.9$ is reached, since $\beta = 3$ is the maximum, and the results are more promising. But the role of λ is not as clear as that of β, all that is known is that the higher the λ, the smaller the length of the displacement vectors [27], so if a sufficiently long λ is achieved, the algorithm will cease to be non-rigid registration and become rigid registration [39].

As Hirose [27] mentions, the tuning parameter λ is difficult to interpret and it tends to be controlled in a non-intuitive manner. Then, the algorithm is tested for different values of λ, increasing from 50 to 400, as seen in Table 2 and results are evaluated with the RMSE to figure out which is the most accurate registration.
In the same table, the RMSE values are not so different from a λ value to another, they vary in decimals and do not follow a very clear pattern either. Following the logic of the algorithm and the λ function definition [27], the smaller the λ, the longer the length of the displacement vectors, so the more accurate the rigid registration and finally, the lower the RMSE between the morphed source and the target. But this is not appreciated, there is not a very definite pattern, and it is seen that the errors are larger as the lambda decreases, which leads to think that perhaps, the optimal lambda is not the smallest one, but another one a little larger.

To be able to compare the initial source and the morphed resultant source, a rigid registration as the one in the first step was made, merely with the intention of aligning both models. If we look at Figures 14 and 15, we see that the main difference between the two models is that the red one, the morphed resultant source, is slightly tilted forward, which makes sense as the patient's femur is more upright vertically.
In addition, it can also be seen that the soft tissues have also undergone a change but there are no initial tissues to compare with as the initial target did not have segmented soft tissues.
So, the only way to see if the result is viable is to test the quality of the morphed resultant mesh. Ideally, the fewer analysis warnings the mesh verification has, the fewer irregularities and the more robust and computable the mesh will be. Results of every mesh verification for every lambda and every patient are shown in Tables 3 to 7. A comparison of the total analysis warnings and in every soft tissue of the original source and each morphed resultant source are shown in each table.

As a first impression, those morphed resulting source models resulting from a non-rigid registration with a small lambda value tend to have more analysis warnings, because the displacement vectors are larger, the model deforms more, and the resulting mesh loses quality.

Finally, it can be said that a good morphed resultant source will be a model that has managed to fit the target geometry well, that is a small RMSE, and that has a computable mesh, that is a low total number of warnings analysis. In Table 8 we have selected the best λ for each patient that minimizes the factors mentioned above and three out of five results have been achieved with λ equal to 400. So, we could conclude that the optimal parameters to obtain a personalized knee model for osteoarthritic patients with the BCPD algorithm is $\lambda = 400$ and $\beta = 2.9$.

6. Conclusion

In conclusion, the presented mesh-morphing algorithm managed to deliver a personalized OA knee model in a fast and straightforward way. The results show that the source model fits the target/patient geometry very well and the resulting mesh is free of irregularities and fully computable.

We can conclude by saying that personalized models seem to be a good substitute for patient-specific models. Moreover, this information can be very helpful to physicians to generate more personalized treatments to delay OA's natural course and at the end, improve patient's quality of life.

Nevertheless, we must bear in mind that the results are only consistent for three of the five outcomes obtained, so the study is a good starting point and that due to lack of time, it has not been possible to test the algorithm for more patients.

So as future directions, the algorithm should be tested on more patients, the results obtained should be studied and fixed parameters common to all registrations should be determined, so that future personalized models can be obtained in a faster and more direct way and computational analyses can be performed with them. Finally, once the personalized 3D models of OA knee joints are obtained, finite element simulations must be performed and studied in order to better understand the progression and the direction in which the pathology is heading.

BIBLIOGRAPHY

[1]. Dahaghin, S. (2005). Prevalence and pattern of radiographic hand osteoarthritis and association with pain and disability (the Rotterdam study). *Annals Of The Rheumatic Diseases*, *64*(5), 682-687. doi: 10.1136/ard.2004.023564

[2]. Hawker G. A. (2019). Osteoarthritis is a serious disease. *Clinical and experimental rheumatology*, *37 Suppl 120*(5), 3–6.

[3]. Shane Anderson, A., & Loeser, R. (2010). Why is osteoarthritis an age-related disease?. *Best Practice &Amp; Research Clinical Rheumatology*, *24*(1), 15-26. doi: 10.1016/j.berh.2009.08.006

[4]. Study the relevance between inflammatory factors and estradiol and their association with knee osteoarthritis in postmenopausal women. (2022). Retrieved 18 June 2022, from https://www.europeanreview.org/article/14197

[5]. Bitton R. (2009). The economic burden of osteoarthritis. *The American journal of managed care*, *15*(8 Suppl), S230–S235.

[6]. Hunter, D., & Bierma-Zeinstra, S. (2019). Osteoarthritis. *The Lancet*, *393*(10182), 1745-1759. doi: 10.1016/s0140-6736(19)30417-9

[7]. Devaraj, Ashwin & Adhikari, Raviraja & Acharya, Kiran & adarshrshetty0204@gmail.com,. (2016). Finite Element Analysis of a Human Knee Joint.

[8]. Etoundi, A., Semasinghe, C., Agrawal, S., Dobner, A., & Jafari, A. (2021). Bio-Inspired Knee Joint: Trends in the Hardware Systems Development. *Frontiers In Robotics And AI*, *8*. doi: 10.3389/frobt.2021.613574

[9]. Vaienti, E., Scita, G., Ceccarelli, F., & Pogliacomi, F. (2017). Understanding the human knee and its relationship to total knee replacement. *Acta bio-medica : Atenei Parmensis*, *88*(2S), 6–16. https://doi.org/10.23750/abm.v88i2-S.6507

[10]. Sophia Fox, A. J., Bedi, A., & Rodeo, S. A. (2009). The basic science of articular cartilage: structure, composition, and function. *Sports health*, *1*(6), 461–468. https://doi.org/10.1177/1941738109350438

[11]. Woods, A., Wang, G., & Beier, F. (2007). Regulation of chondrocyte differentiation by the actin cytoskeleton and adhesive interactions. *Journal of cellular physiology*, *213*(1), 1–8. https://doi.org/10.1002/jcp.21110

[12]. Xia, B., Di Chen, Zhang, J., Hu, S., Jin, H., & Tong, P. (2014). Osteoarthritis pathogenesis: a review of molecular mechanisms. *Calcified tissue international*, *95*(6), 495–505. https://doi.org/10.1007/s00223-014-9917-9

[13]. Jalalvand, A., Anbarian, M., Ahanjan, S., Hajiloo, B., & Tayfe Seyedan, A. (2017). The Effect of Knee Osteoarthritis on Excursions of Lower Limb Joints During Gait. *Physical Treatments - Specific Physical Therapy*, *6*(4), 233-241. doi: 10.18869/nrip.ptj.6.4.233

[14]. Shane Anderson, A., & Loeser, R. F. (2010). Why is osteoarthritis an age-related disease?. *Best practice & research. Clinical rheumatology*, *24*(1), 15–26. https://doi.org/10.1016/j.berh.2009.08.006

[15]. Litwic, A., Edwards, M., Dennison, E., & Cooper, C. (2013). Epidemiology and burden of osteoarthritis. *British Medical Bulletin*, *105*(1), 185-199. doi: 10.1093/bmb/lds038

[16]. Nguyen, U. S., Zhang, Y., Zhu, Y., Niu, J., Zhang, B., & Felson, D. T. (2011). Increasing prevalence of knee pain and symptomatic knee osteoarthritis: survey and cohort data. *Annals of internal medicine*, *155*(11), 725–732. https://doi.org/10.7326/0003-4819-155-11-201112060-00004

[17]. Vos, T., Allen, C., Arora, M., Barber, R., Bhutta, Z., & Brown, A. et al. (2016). Global, regional, and national incidence, prevalence, and years lived with disability for 310 diseases and injuries, 1990–2015: a systematic analysis for the Global Burden of Disease Study 2015. *The Lancet*, *388*(10053), 1545-1602. doi: 10.1016/s0140-6736(16)31678-6

[18]. SINUSAS, K. (2022). Osteoarthritis: Diagnosis and Treatment. Retrieved 2 June 2022, from https://www.aafp.org/pubs/afp/issues/2012/0101/p49.html

[19]. Expert Guide to Rheumatology Arthur Yee Expert Guide to Rheumatology , Stephen Paget American College of Physicians No of pages: 500 £31.95 1930513 550 1930513550 [Formula: see text]. (2005). *Nursing older people*, *17*(9), 35. https://doi.org/10.7748/nop.17.9.35.s22

[20]. Lespasio, M. J., Piuzzi, N. S., Husni, M. E., Muschler, G. F., Guarino, A., & Mont, M. A. (2017). Knee Osteoarthritis: A Primer. *The Permanente journal*, *21*, 16–183. https://doi.org/10.7812/TPP/16-183

[21]. Paz, A., Orozco, G., Korhonen, R., García, J., & Mononen, M. (2021). Expediting Finite Element Analyses for Subject-Specific Studies of Knee Osteoarthritis: A Literature Review. *Applied Sciences*, *11*(23), 11440. doi: 10.3390/app112311440

[22]. Kazemi, M., Dabiri, Y., & Li, L. (2013). Recent Advances in Computational Mechanics of the Human Knee Joint. *Computational And Mathematical Methods In Medicine*, *2013*, 1-27. doi: 10.1155/2013/718423

[23]. Cooper, R. J., Wilcox, R. K., & Jones, A. C. (2019). Finite element models of the tibiofemoral joint: A review of validation approaches and modelling challenges. *Medical engineering & physics*, *74*, 1–12. https://doi.org/10.1016/j.medengphy.2019.08.002

[24]. Sigal, I. A., Hardisty, M. R., & Whyne, C. M. (2008). Mesh-morphing algorithms for specimen-specific finite element modeling. *Journal of biomechanics*, *41*(7), 1381–1389. https://doi.org/10.1016/j.jbiomech.2008.02.019

[25]. What is Mesh Morphing | IGI Global. (2022). Retrieved 2 June 2022, from https://www.igi-global.com/dictionary/mesh-morphing-smoothing-means-radial/18339

[26]. Point Set Registration Methods—Discussion and Implementation. (2022). Retrieved 2 June 2022, from https://medium.com/swlh/point-set-registration-methods-discussion-and-implementation-58efa98d0b68

[27]. Hirose, O. (2021). A Bayesian Formulation of Coherent Point Drift. *IEEE Transactions On Pattern Analysis And Machine Intelligence*, *43*(7), 2269-2286. doi: 10.1109/tpami.2020.2971687

[28]. Weng Jiang, Y. (2019). Morphing operations for the adaptation of structural finite element meshes to patient-specific knee joint geometries. Bachelor Thesis from University Pompeu Fabra

[29]. Besl, P., & McKay, N. (1992). A method for registration of 3-D shapes. *IEEE Transactions On Pattern Analysis And Machine Intelligence*, *14*(2), 239-256. doi: 10.1109/34.121791

[30]. Zhang, Z. (1994). Iterative point matching for registration of free-form curves and surfaces. *International Journal Of Computer Vision*, *13*(2), 119-152. doi: 10.1007/bf01427149

[31]. Jana, P., & Dalibor, M. (2018). Notes on iterative closest point algorithm

[32]. Bookstein, F. (1989). Principal warps: thin-plate splines and the decomposition of deformations. *IEEE Transactions On Pattern Analysis And Machine Intelligence*, *11*(6), 567-585. doi: 10.1109/34.24792

[33]. Erdemir A. Open Knee: Open Source Modeling and Simulation in Knee Biomechanics. J Knee Surg. 2016 Feb;29(2):107-16. doi: 10.1055/s-0035-1564600. Epub 2015 Oct 7. PMID: 26444849; PMCID: PMC4876308.

[34]. Chen, A. (2022). 5 vital things to know about STL file format in 3D printing. Retrieved 2 June 2022, from https://www.cmac.com.au/blog/5-vital-things-about-stl-file-format-3d-printing

[35]. 2. The VTK file format — VisIt User Manual 3.1 documentation. (2022). Retrieved 2 June 2022, from https://visit-sphinx-github-user-manual.readthedocs.io/en/task-allen vtk9_master_ospray/data_into_visit/VTKFormat.html

[36]. Chui, H., & Rangarajan, A. (2003). A new point matching algorithm for non-rigid registration. *Computer Vision And Image Understanding*, *89*(2-3), 114-141. doi: 10.1016/s1077-3142(03)00009-2

[37]. Maiseli, B., Gu, Y., & Gao, H. (2017). Recent developments and trends in point set registration methods. *Journal Of Visual Communication And Image Representation*, *46*, 95-106. doi: 10.1016/j.jvcir.2017.03.012

[38]. Hirose, O. (2021). Acceleration of Non-Rigid Point Set Registration With Downsampling and Gaussian Process Regression. *IEEE Transactions On Pattern Analysis And Machine Intelligence*, *43*(8), 2858-2865. doi:10.1109/tpami.2020.3043769

[39]. GitHub - ohirose/bcpd: Bayesian Coherent Point Drift (BCPD/BCPD++). (2022). Retrieved 2 June 2022, from https://github.com/ohirose/bcpd

[40]. ABAQUS/CAE User's Manual (v6.6). (2022). Retrieved 10 June 2022, from https://classes.engineering.wustl.edu/2009/spring/mase5513/abaqus/docs/v6.6/books/usi/default.htm?startat=pt03ch17s06s01.html

[41]. Harrington IJ. A bioengineering analysis of force actions at the knee in normal and pathological gait. Biomed Eng. 1976;11(5):167–72.

[42]. Prendergast P. J. (1997). Finite element models in tissue mechanics and orthopaedic implant design. *Clinical biomechanics (Bristol, Avon)*, *12*(6), 343–366. https://doi.org/10.1016/s0268-0033(97)00018-1

[43]. Wismans, J., Veldpaus, F., Janssen, J., Huson, A., & Struben, P. (1980). A three-dimensional mathematical model of the knee-joint. *Journal Of Biomechanics*, *13*(8), 677-685. doi: 10.1016/0021-9290(80)90354-1

[44]. morphing, M. (2022). AdSimuTec - Preprocessing: Use of mesh morphing for model variation. Retrieved 18 June 2022, from https://adsimutec.com/en/fem-cfd-simulation-engineering-services/preprocessing-modeling/mesh

[45]. Chan, D., Cai, L., Butz, K. *et al. In vivo* articular cartilage deformation: noninvasive quantification of intratissue strain during joint contact in the human knee. *Sci Rep* **6,** 19220 (2016). https://doi.org/10.1038/srep19220

[46]. Huiskes, R., & Chao, E. Y. (1983). A survey of finite element analysis in orthopedic biomechanics: the first decade. *Journal of biomechanics*, *16*(6), 385–409. https://doi.org/10.1016/0021-9290(83)90072-6

[47]. A. Myronenko and X. Song, "Point set registration: Coherent point drift," IEEE Transactions on Pattern Analysis and Machine Intelligence, vol. 32, no. 12, pp. 2262–2275, 2010

[48]. Saiti, E., Danelakis, A., & Theoharis, T. (2021). Cross-time registration of 3D point clouds. *Computers &Amp; Graphics*, *99*, 139-152. doi: 10.1016/j.cag.2021.07.005

[49]. Papaioannou, G., Nianios, G., Mitrogiannis, C., Fyhrie, D., Tashman, S., & Yang, K. H. (2008). Patient-specific knee joint finite element model validation with high-accuracy kinematics from biplane dynamic Roentgen stereogrammetric analysis. *Journal of biomechanics*, *41*(12), 2633–2638. https://doi.org/10.1016/j.jbiomech.2008.06.027